Article ID: 1006-8775(2020) 03-0311-10

A New Index About the Walker Circulation

SHI Dan-dan (石丹丹) [1], RONG Yan-shu (荣艳淑) [1,2], LYU Xing-yue (吕星玥) [1], WU Fu-ting (吴福婷) [1,2]
(1. College of Hydrology and Water Resources, Hohai University, Nanjing 210098 China;
2. The Experimental Teaching Center of Water Conservancy Projects of Hohai University, Nanjing 210098 China)

Abstract: The Walker circulation (WC) has always been an important issue in atmospheric science research due to the association between the WC and tropical Pacific sea surface temperature (SST), and between the WC and ENSO events. In this paper, a new index-Omega index (OMGI)-is constructed for WC characterization based on the NCEP/NCAR reanalysis data of monthly mean vertical velocity in recent 70 years (1948−2017). Results show that the OMGI can accurately depict the variation characteristics of WC on seasonal, annual and decadal time-scales. There is a significant inverse correlation between the OMGI and equatorial eastern and central Pacific SST. Meanwhile, the peak of the OMGI appears ahead of the ENSO peak, and therefore is able to reflect the SST in the equatorial Pacific. Especially, in 35 ENSO events, the peak of the OMGI appears earlier than Niño 3.4 index for 19 times with 2.6 months ahead on average. In 16 El Niño events, the peak of the OMGI occurs ahead of the El Niño for 9 times with 4 months ahead on average. In 19 La Niña events, the OMGI peak arises 10 times earlier than the La Niña peak, with an average of 1.4 months ahead. OMGI shows obvious leading effect and stability over ENSO events with different strengths and types of single peak and multi peaks: the peak of the OMGI keeps about 2−3 months ahead of the ENSO. Compared with other WC indexes such as UWI and SPLI, OMGI has some advantages in the ability to describe WC changes and present the probability and the time of prediction of ENSO event peaks.

Key words: Walker circulation; OMGI; Niño 3.4; UWI; SLPI
CLC number: P447 **Document code:** A
https://doi.org/10.16555/j.1006-8775.2020.028

1 INTRODUCTION

The temperature difference between the east and west of the tropical ocean promotes the development of atmospheric zonal circulation. The zonal circulation perpendicular to the sea level is formed over the tropical Indian Ocean, the tropical Pacific and the tropical Atlantic (Hastenrath [1]). Among them, the Walker circulation (WC) spans the entire tropical Pacific ocean and consists of the updraft (ascending branch) over the equatorial western Pacific, the westerly wind near the tropopause, the downdraft (descending branch) over the equatorial eastern Pacific and the northeast trade wind blowing westward in the lower troposphere (Gill [2]).

The WC is generated due to the heating of the western Pacific warm pool to the atmosphere, and in turn it affects the equatorial Pacific sea surface temperature (SST). Therefore, there is an interaction and feedback between the WC and SST (Yang and Chen [3]). When the eastern Pacific is warmer than normal, indicating the occurrence of El Niño, the strength of the warm pool in the western Pacific weakens and then the WC weakens. Thus, the ascending and descending branches of the WC move eastward. Conversely, when SST in the eastern Pacific declines, indicating the occurrence of La Niña, the WC grows and then the ascending and descending branches of the WC shift westward (Bayr et al. [4]; Han et al. [5]). As the air flow moves upward in the ascending branch of the WC and downward in the descending branch, the weather and climate in the areas controlled by the ascending and descending branches of the WC are obviously different. In the ascending branch of the WC, a large amount of warm and wet air over the ocean surface is transported to the middle troposphere, causing more precipitation over land and the western Pacific. While in the descending branch of the WC, no water vapor is raised and the climate is dry with less precipitation. In the area where the ascending branch of the WC strengthens, convection is stronger, leading to a increase of precipitation. However, in the area where the descending branch strengthens, it becomes drier (Sohn et al. [6]). Therefore, the change of the WC will cause significant changes in precipitation intensity and distribution, leading to the occurrence of extreme weather events, which will have an impact on human society (Oliveira et al. [7]; Yim et al. [8]; Sasaki et al. [9]).

Some studies showed that the WC can change the

Received 2019-07-20; **Revised** 2020-05-15; **Accepted** 2020-08-15

Funding: National Natural Science Foundation of China (41605043); National Key R&D Program of China (2016YFA0601504); Fundamental Research Funds for the Central Universities (2017B00114)

Biography: SHI Dan-dan, M. D., primarily undertaking research on hydrometeorology and hydroclimatology.

Corresponding author: RONG Yan-shu, e-mail: ysron@hhu.edu.cn

SST in the central and eastern equatorial Pacific (Bjerknes [10, 11]; Philander [12]; Wyrtki [13]). As the most significant signal, the occurrence and development of ENSO events have a great impact on global weather and climate, and may even cause disastrous weather in the coming months in many places (Wang et al. [14]). Therefore, the research of ENSO has always been a hot topic in meteorology. Many researches on ENSO prediction have been carried out; for example, the the extratropical cyclone activity has become the key to improve ENSO long-term predictive technology (Anderson [15]; Tasambay-Salazar et al. [16]). Wang et al. [17] confirmed the influence of Rossby wave propagation in temperate regions during the transition from El Niño to La Niña and Wang [18] proposed the atmospheric circulation system over mid latitude may be the original external force of ENSO events. In fact, there are two types of El Niño, i.e., traditional El Niño event and El Niño Modoki event, in the equatorial Pacific (Weng et al. [19]; Zhang et al. [20]; Zhi et al. [21], Wang et al. [22]) and the impact of El Niño Modoki events on the climate is different from that of traditional El Niño events. Therefore, the research of ENSO prediction technology is still important.

The WC is closely related to ENSO events and there is a strong relationship between Walker circulation and ENSO in annual time scale (Sun et al. [23]). Some studies showed that the WC can change the SST in the central and eastern equatorial Pacific, indicating that the WC may change before ENSO (Bo and Wu [24]; Ma and Zhang [25]). Bo and Wu [24] pointed out that the change of the WC is 2–3 months ahead of the eastern equatorial Pacific SST variation. Some other studies suggested that the weakening tropical trade wind brings SST anomalies in equatorial Pacific, which induces ENSO events (Bjerknes [11]; Philander [12]; Wyrtki [13]). These studies confirmed that the WC may appear ahead of ENSO events.

In conclusion, the change of WC can indicate the occurrence of ENSO, and it plays an important role in precipitation prediction and disaster warning. Therefore, in this paper, a new WC index with better leading effect on ENSO events is constructed, and its feasibility is also discussed.

2 DATA AND INDEXES

The data used in this paper include monthly zonal wind speed and vertical velocity (Omega) from NCEP/NCAR, and sea surface temperature (SST) from NOAA. The spatial resolution of SST is 2°×2°, and it is 2.5°×2.5° for the others. The time range is from 1948 to 2017.

2.1 *ENSO index*

Niño 3.4 index is adopted as ENSO monitoring index (Smith et al. [26]). Niño 3.4 index is the average SST anomaly over 5° S–5° N, 170° W–120° W (Fig. 1, black square frame). Climate base period is from 1981 to 2010. An ENSO event occurs when the absolute value of the three-month running average of Niño 3.4 index reaches or exceeds ±0.5℃, and maintains for at least 5 months. The time when the absolute value of the three-month running average of Niño 3.4 index reaches the maximum and the value during this time are defined as the peak time and peak intensity of the event, respectively. When there are more than one peak with the same intensity in any event, the first peak shall prevail. The peak intensity of the event is selected to represent the intensity of the event. According to the classification rules shown in Table 1, 35 ENSO events are extracted during 1948–2017, among which 16 are El Niño events and 19 are La Niña events. More detailed information of ENSO events is summarized in Table 2. There are 7 strong ENSO events, 12 medium events and 16 weak events.

2.2 *Walker circulation indexes*

The commonly used WC indexes include the zonal wind index (UWI) in the equatorial Pacific (Zhang and Li [27, 28]; Yue and Xu [29]), the sea level pressure index (SLPI) between the eastern and western Pacific (Sun et al. [22]), and the zonal mass flux flow function (Bayr et al. [4]; Yue and Xu [29]). Here, the UWI (Yue and Xu [29]) and the SLPI (Sun et al. [23]) are compared with the new WC index established in this paper. The two indexes are defined as follows:

$$\mathrm{UWI} = u_{200} - u_{850} \quad (1)$$

In Eq. (1), u_{200} and u_{850} are average zonal wind at 200 hPa and 850 hPa over the region of 5°S–5°N, 160°E–100°W (Fig. 1, orange area).

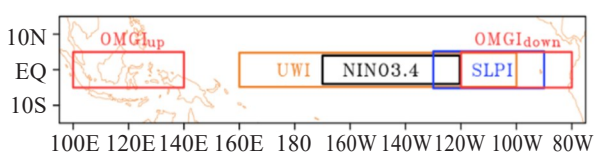

Figure 1. Definitions of the Niño 3.4 (4°S – 4°N, 170°W – 120°W), UWI (5°S – 5°N, 160°E – 100°W), SLPI (5°S – 5°N, 130°W – 90°W and 140°E – 180°), and Omega index (OMGI).

$$\mathrm{SLPI} = \mathrm{slp}_1 - \mathrm{slp}_2 \quad (2)$$

In Eq. (2), slp_1 and slp_2 are average sea surface pressure over region 1 (5° S–5° N, 130° W–90° W) and region 2 (5° S–5° N, 140° E–180°), respectively (Fig. 1, two blue square frames).

3 OMEGA INDEX AND ITS CHANGES

3.1 *Construction of Omega index (OMGI)*

Figure 2a shows the composite wind of zonal divergent wind and vertical velocity ω to draw the height-longitude profile of zonal vertical circulation over equatorial Pacific and the variance of vertical velocity. It is clear that the updraft is located on the west side of 160° W and the downdraft on the east side along with the tropopause westerly winds and surface easterly trade winds, forming a complete and closed circulation over the equatorial Pacific.

Table 1. The classification of ENSO events.

	Strong event	Medium event	Weak event
El Niño	Niño 3.4≥2	1.3≤Niño 3.4 < 2	0.5≤Niño 3.4 < 1.3
La Niña	Niño 3.4≤−2	−2 < Niño 3.4≤−1.3	−1.3 < Niño 3.4≤−0.5

Table 2. ENSO events during 1948–2017.

El Niño events	Time	Niño 3.4 peak value	Intensity level	La Niña events	Time	Niño 3.4 peak value	Intensity level
1	1957.5−1958.6	1.5	Medium	1	1948.7−1951.4	−1.9	Medium
2	1963.9−1964.2	0.9	Weak	2	1954.5−1957.2	−2.2	Strong
3	1965.7−1966.4	1.4	Medium	3	1959.8−1959.12	−0.8	Weak
4	1968.12−1969.5	0.9	Weak	4	1961.9−1963.3	−0.9	Weak
5	1972.7−1973.3	2.0	Strong	5	1964.5−1965.3	−1.4	Medium
6	1976.11−1977.3	0.7	Weak	6	1966.12−1968.5	−0.9	Weak
7	1982.6−1983.7	2.2	Strong	7	1970.7−1972.3	−1.5	Medium
8	1986.10−1988.2	1.5	Medium	8	1973.6−1976.6	−2.2	Strong
9	1991.7−1992.7	1.8	Medium	9	1978.5−1978.11	−0.6	Weak
10	1994.8−1995.4	1.2	Weak	10	1983.10−1985.11	−1.2	Weak
11	1997.6−1998.6	2.4	Strong	11	1988.6−1989.8	−2.0	Strong
12	2002.6−2003.3	1.4	Medium	12	1995.9−1996.4	−0.9	Weak
13	2004.8−2005.3	0.8	Weak	13	1998.8−2001.4	−1.7	Medium
14	2006.10−2007.2	1.0	Weak	14	2005.12−2006.4	−0.8	Weak
15	2009.8−2010.4	1.6	Medium	15	2007.8−2008.7	−1.6	Medium
16	2014.11−2016.6	2.7	Strong	16	2008.12−2009.4	−0.8	Weak
				17	2010.7−2011.5	−1.6	Medium
				18	2011.9−2012.4	−1.0	Weak
				19	2016.9−2017.1	−0.7	Weak

In addition, the ascending branch has several strong rising centers. The strongest rising center locates near 150° E where the ascending motion rises from the 900 hPa to the tropospheric top. The second strongest rising center is located near 110° E, with similar but much smaller intensity to the strongest one. The third and fourth strongest rising centers are located around 100° E and 90° E, respectively, with smaller intensity and range compared with the second. The descending branch which is distributed along 140° W–80° W only has one sinking center extending from 120° W to 80° W. The subsidence center has a large area, but its strength is less than that of the ascending center. In addition, the ascending branch can rise from 900 hPa to 200 hPa and its width can extend westward from 180° to 80° E. Near 600 hPa its east boundary can reach 160° W. The descending branch starting from 200 hPa only reaches 800 hPa, and then it turns into easterly trades. Therefore, the longitude range and vertical height of the ascending branch are larger than those of the descending branch, and it is the same with the intensity.

Figure 2b shows the variance distribution of the vertical velocity during the period of 1948–2017. There are three regions between 300 hPa and 400 hPa with the greatest variance of vertical velocity: one is around 160° W–170° W (roughly at the boundary between ascending and descending branches), one is near 130°E (between the first and second strongest rising center), and one is near 110° E. Among them, the variances around 130°E and 160°W–170°W are the largest.

According to the principle of maximum vertical velocity variance in the updraft zone and stable vertical velocity in the downdraft zone, the vertical velocity in ascending region and descending region is selected to construct a new WC index—OMGI to characterize the intensity variation of the WC. The form of the OMGI is as follows:

$$\mathrm{OMGI} = \omega_{\mathrm{up}} - \omega_{\mathrm{down}} \quad (3)$$

In Eq. (3), ω_{up} and ω_{down} represent the mean vertical velocity of the ascending branch area (100° E–140° E) and the descending branch area (120° W–80° W) over 5° S–5° N, 850 hPa–200 hPa (Fig. 1, red square frames). The OMGI calculated by Eq. (3) is the three-month running averaged and standardized with the mean value of 0 and the variance of 1. When ω is positive, it represents ascending motion. While ω is negative, it represents descending motion. ω_{up} is positive because ω with positive sign represents ascending motion. Similarly, ω_{down} is negative. Thus, when the OMGI is positive, the descending motion is significantly

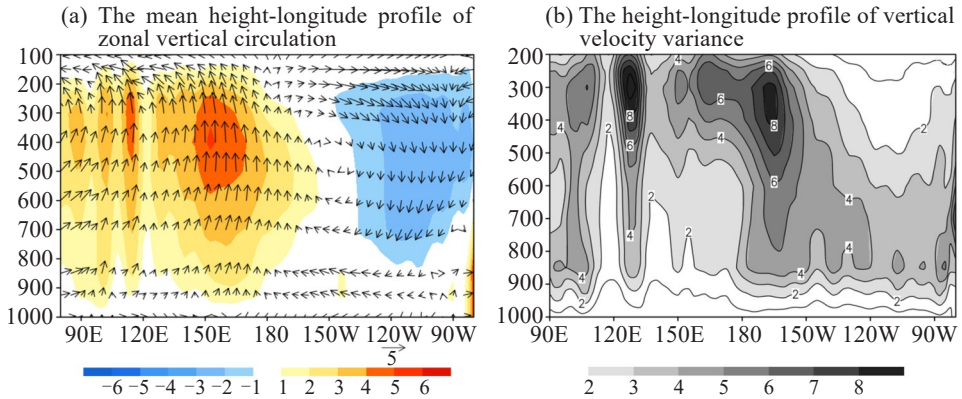

Figure 2. (a) The mean height-longitude profile of average zonal vertical circulation over equatorial Pacific from 5° S−5° N. The arrows are composite of zonal divergent wind (m s^{-1}) and vertical velocity (0.01Pascal s^{-1}). Shadows represent the intensity of vertical velocity. The red shadows are the ascending areas and the blue shadows are the descending areas. (b) The height-longitude profile of average vertical velocity variance over 5°S−5°N.

enhanced, corresponding to La Niña events. When the OMGI is negative, the ascending motion is significantly weakened, corresponding to El Niño events.

3.2 *Seasonal variation of the WC reflected by the OMGI*

Figure 3 reveals the seasonal variation of the WC and the OMGI. The vertical velocity is magnified 100 times. The red shadows are the ascending areas and the blue shadows are the descending areas. From January-February, the updraft expands from 160° W to 80° E and the ascending velocity is very high with several rising centers. The downdraft appears between 140° W and 90°W and the descending velocity is relatively low. Between March and May, the updraft weakens, and the strong rising centers narrows. However, the range of the ascending branch extends eastward obviously, especially in April, with the eastern boundary of the ascending branch reaching 130° W. The downdraft also weakens, and the sinking velocity reaches the minimum. After June, the updraft strengthens but its eastern boundary retreats significantly to the west. The rising centers begin to strengthen and expand. At the same time, the downdraft strengthens too, while its range is still relatively small. In July, the strong rising center from 150° E−180° reaches its maximum and starts to weaken, and the rising centers between 100° E−120° E are still weak and keep growing. The intensity of sinking motion is the strongest in September and the range is the largest in October. After November, the strong rising centers between 100° E and 120° E continues to grow strongly. Meanwhile, the strong rising center between 150° E and 180° enhances again and the downdraft gradually weakens. Therefore, the locations and intensities of the ascending branch and the descending branch of the WC vary in different seasons. The ascending branch is the strongest in spring, and the weakest in winter, whereas the descending branch is the weakest in spring, and the strongest in autumn.

As shown in Fig. 3b, the OMGI is the largest in January, and decreases gradually. Its value is relatively low from April-June and reaches the lowest in May. The OMGI increases gradually after September and finally reaches its maximum in December. This phenomenon is very similar to the results in Fig. 2b, which indicates that the value of the OMGI is higher in winter and lower in spring; this result is consistent with the WC.

3.3 *The decadal change of the WC reflected by the OMGI*

Figure 4 shows the height-longitude profile of the WC with decadal mean in which the 2010s is replaced by the mean of 2011−2017. The range and intensity of

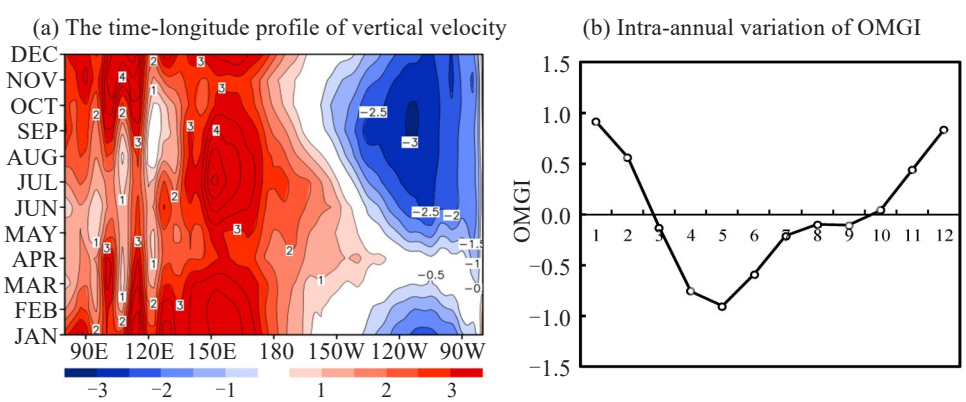

Figure 3. (a) The time-longitude profile of average vertical velocity (0.01Pascal s^{-1}) over 5°S−5°N, 850 hPa−200 hPa during 1948−2017; (b) the intra-annual variation of the OMGI.

the ascending and descending branches of the WC vary in different decades. In terms of range, the ascending branches in the 1950s (Fig. 4a) and 1960s (Fig. 4b) are larger than normal, extending from 80°E to 150°W and occupying 130 longitudes, while the ascending branches in other decades cover a range of 100−110 longitudes. It is worth noting that in the 2010s, although the longitude range of the ascending branch does not expand significantly, the updraft rises from the sea surface, enlarging the height range of the ascending motion obviously. Descending branch dominates between 80°W − 135° W from the 1950s (Fig. 4a) to the 1980s (Fig. 4d). After the 1990s (Fig. 4e), the range of descending branch is narrower and extends upward. In the 2010s, the descending branch extends to the sea level and breaks. The strength of ascending branch from the 1950s−1990s (Fig. 4a-e) continues to weaken, and then increases rapidly in the 2000s and 2010s (Fig. 4f-g), exceeding that in the 1950s. The strength of descending branch also continues to weaken from the 1950s to the 1990s (Fig. 4a-e), and increases after the 20th century, but does not exceed the strength of that in the 1980s (Fig. 4d). Therefore, the WC from the 1950s to the 1990s is weak and its dominating range is relatively

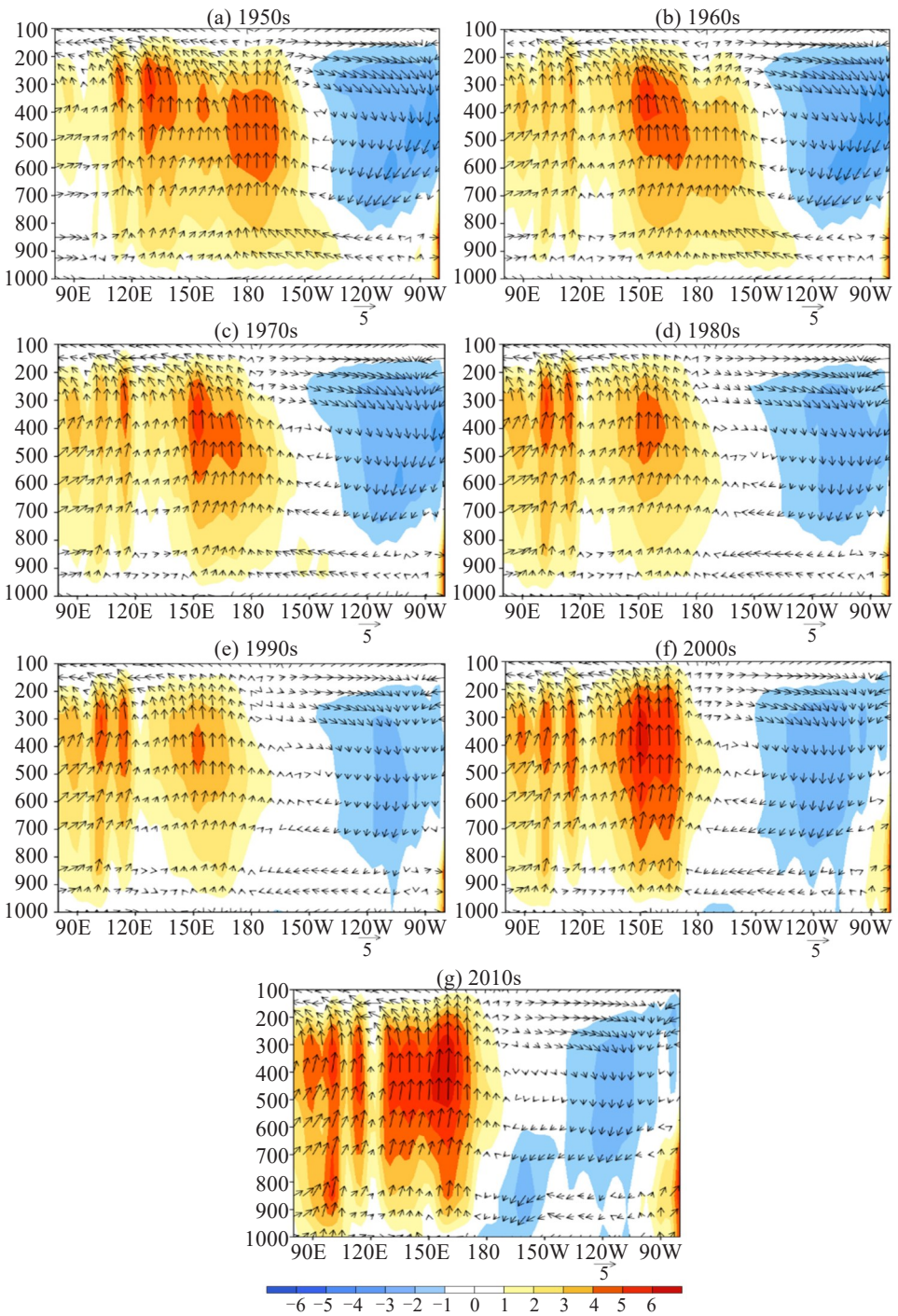

Figure 4. The same as that in Fig. 2a, but with the decadal mean; a−g represent the 1950s−2010s, respectively.

small, while in the 2000s and the 2010s it is stronger, and its dominating range is larger. The enhancement of the WC is consistent with the views of Sohn et al. [30], Bayr et al. [4] and Sun and Li [31].

According to the time series of the monthly OMGI (Fig. 5), the OMGI fluctuation amplitude before the 1980s is small and it fluctuates between ± 2 in most periods, basically corresponding to the phenomenon in Fig. 4a-c. In the 1980s and 1990s, the OMGI shows a strong negative fluctuation period corresponding to the weakening of ascending and descending branches of the WC in Fig. 4d-e. In the 21st century, the occurrence and intensity of positive amplitude gradually increase, while those of negative amplitude weaken, corresponding to the phenomenon of the WC enhancement in Fig. 4f-g. Therefore, according to the temporal evolution rule shown in Fig. 5, the OMGI can basically reflect the decadal variations of the WC.

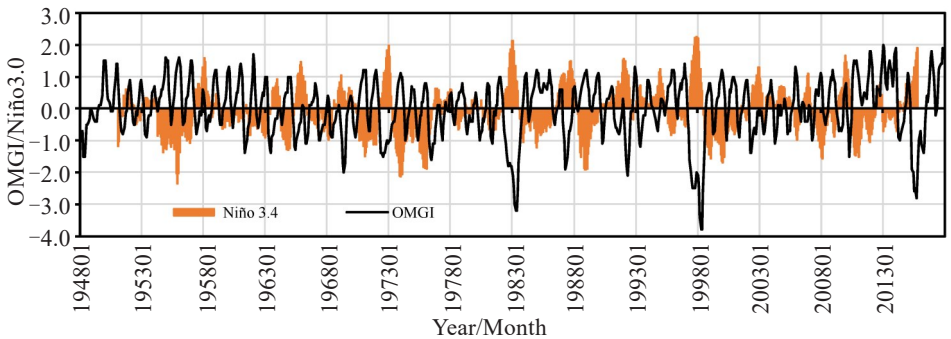

Figure 5. The time series of the OMGI and Niño 3.4.

3.4 *Relationship between the OMGI and equatorial Pacific SST*

Figure 5 shows the time variation of monthly Niño 3.4 index and the OMGI. The OMGI and Niño 3.4 index exhibit opposite variations with a negative correlation coefficient of −0.51. It corresponds with the distribution of correlation coefficients between the OMGI and SST in Fig. 6, which reveals that the OMGI has a significant negative correlation with the SSTs in equatorial central and eastern Pacific. Negative Niño 3.4 index represents low SST in the equatorial eastern Pacific. It means that when the SST in the equatorial western Pacific is high, it promotes the upward movement of the atmosphere over the western Pacific, and the WC is strong. Therefore, the OMGI is in the positive phase. Conversely, when Niño 3.4 index is in the positive phase, it shows that the SST in the equatorial eastern Pacific is higher, while the SST in the equatorial western Pacific is lower. The WC weakens and the OMGI is in its negative phase. This conclusion is consistent with that of Yuan et al. [32], Zhang and Li [33], and Ana et al. [34]. Therefore, the OMGI constructed in this paper not only can reflect the characteristics of seasonal and interannual variations of the WC, but also has inverse change of SST in the equatorial eastern Pacific, which indicates that the OMGI can reasonably represent the WC.

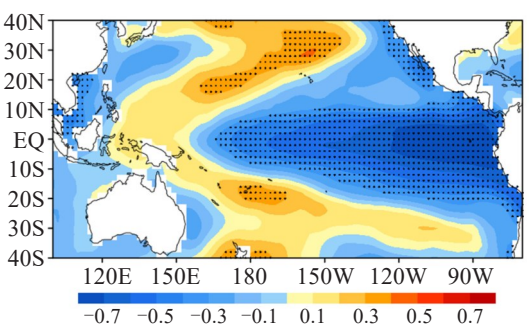

Figure 6. The correlation coefficients between the OMGI and SST (the black spot representing the areas passing the significant test of 99.9%).

4 THE COMPARISONS BETWEEN OMGI AND OTHER WC INDEXES

4.1 *Intra-annual and inter-annual variation of the WC based on three indexes*

In order to understand the similarities and differences between the OMGI and other WC indexes, the OMGI is compared with UWI and SLPI indexes. Fig. 7 shows the intra-annual variation of the three indexes. The seasonal variations of the three indexes are all characterized by "single peak". The largest differences among the three indexes are the appearing time of the peaks and the speeds of weakening and growth. The SLPI and the OMGI have similar variation rules, both reaching the peak in winter and the nadir in spring. Their difference mainly lies in the speed that they rebound after spring. The difference between the UWI and the OMGI is obvious. The WC described by UWI reaches its maximum in February and its minimum in September, which is obviously different from the phenomena shown in Fig. 3a.

Figure 8 shows the inter-annual and decadal variations of the three indexes. The UWI reaches its maximum in the 1970s and the minimum in the 1990s. The strength in the 2000s and the 2010s are close to zero (Fig. 8a). Therefore, the variation of UWI does not reflect the decadal variation of the WC in Fig. 4. The decadal average of SLPI shows that the SLPI variation is unobvious during the 1950s and 1990s, which fluctuates

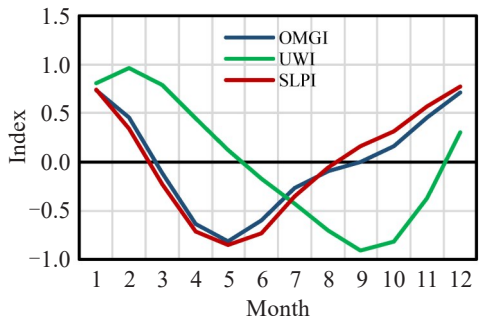

Figure 7. The intra-annual variation of the three WC indexes.

near zero (Fig. 8b). It is relatively small in the 1990s, reaches its maximum in the 2000s and then falls below zero in the 2010s. Therefore, the characteristics of SLPI also do not reflect the enhancement of the WC in the 21st century as shown in Fig. 4.

The decadal variability of the OMGI reaches its maximum in the 1950s and then decreases continuously, reaching its minimum in the 1990s. From the beginning of the 21st century, the decadal mean begins to increase and again exceeds zero in the 2010s (Fig. 8c), indicating that the WC has strengthened since the 21st century. Therefore, the OMGI basically reflects the variation characteristics of the WC in Fig. 2b, but it could not accurately reflect the enhanced intensity in the 21st century. A comprehensive comparison of the indexes in Fig. 8 shows that the OMGI is better than the UWI and the SLPI in depicting the characteristics of WC, although it cannot depict the characteristics accurately either.

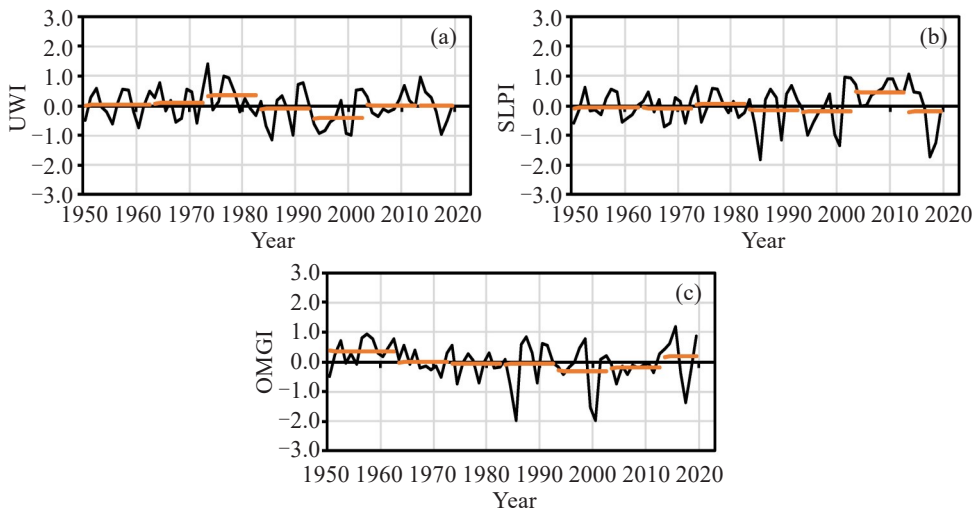

Figure 8. The inter-annual variation of WC represented by (a) the UWI; (b) the SLPI; (c) the OMGI. The orange line represents the decadal mean.

4.2 *Leading effect of the OMGI*

As shown in Fig. 5, the OMGI occurs generally ahead of Niño 3.4. Some studies have also found that WC anomalies generally happen earlier than ENSO (Bo and Wu [24]; Ma and Zhang [25]). Therefore, once the advance time of WC is determined, ENSO can be predicted.

To determine the lead time of the OMGI, UWI and SLPI, the time when the minimum (maximum) of these three indexes appears in strong, medium and weak El Niño (La Niña) events are counted. Then it is compared with the time when the peak of Niño 3.4 index appears, and the number of lead and lag months is obtained (Table 3). When the ENSO event lasts for a long time, the indexes usually show multiple peaks or troughs. In that case, the highest peak or trough value of Niño 3.4 index is taken as representative to discuss the number of months leading or lagging WC indexes. At the same time, Table 3 also shows statistics on the events with a single peak and multi-peaks.

According to Table 3, among the 35 ENSO events, the OMGI gets ahead of Niño 3.4 for 19 times, which is the largest number among those of the three indexes. When it comes to El Niño or La Niña events, the UWI leads El Niño for 14 times in all the 16 events, which is higher than those of the other two indexes. The OMGI leads La Niña for 10 times in all the 19 events, which is more than those of the other two indexes. The average lead months of the three indexes are quite different. The most obvious one is that for El Niño events. The UWI is 2−3 months ahead, while SLPI and the OMGI are about 4 months ahead; while for La Niña events, the lead months of the three indexes are similar. The UWI and the OMGI have longer lead times than the SLPI does when different intense levels of events are discussed. The leading months of UWI, SLPI and OMGI fluctuate between 3.2−1.4, 4.5−1.0, and 2.0−3.0, respectively, indicating that the OMGI is more stable. For single-peak ENSO events, the lead times of UWI and OMGI are close, exceeding that of the SLPI. For multi-peak ENSO events, the OMGI shows the advantage in terms of lead time again. For the number of months ahead, the three

Table 3. The summary of times and months of WC leading or lagging ENSO events. The first column is the classification of ENSO events, and the number in parentheses represent the occurrences of such events.

Event type	Indices	Lead times	Average lead months	Synchronous times	Lag times	Average lag months
ENSO events (35 times)	UWI	17	2.4	4	14	2.4
	SLPI	11	2.8	3	21	2.4
	OMGI	19	2.6	2	14	2.9
El Niño events (16 times)	UWI	14	2.6	1	1	3.0
	SLPI	5	4.2	0	11	2.6
	OMGI	9	4.0	1	6	3.7
La Niña events (19 times)	UWI	3	1.0	3	13	2.3
	SLPI	6	1.7	3	10	2.1
	OMGI	10	1.4	1	8	2.4
Strong events (7 times)	UWI	4	2.8	2	1	1.0
	SLPI	2	1.0	0	5	1.6
	OMGI	3	3.0	1	3	3.0
Medium events (12 times)	UWI	6	3.2	1	5	1.6
	SLPI	4	4.5	2	6	1.8
	OMGI	8	3.1	0	4	3.3
Weak events (16 times)	UWI	7	1.4	1	8	3.0
	SLPI	5	2.2	1	10	3.1
	OMGI	8	2.0	1	7	2.7
Single-peak events (22 times)	UWI	12	2.5	1	9	2.6
	SLPI	4	2.8	2	16	2.4
	OMGI	10	2.5	1	11	2.9
Multi-peak events (13 times)	UWI	5	2.0	3	5	2.0
	SLPI	7	2.9	1	5	2.2
	OMGI	9	2.8	1	3	3.0

indexes are close, which all fluctuate between 2 and 3 months.

Comprehensive comparison results show that the UWI and the OMGI have longer lead times for El Niño and La Niña events, and the number of lead months is stable. In addition, the UWI and the OMGI are still advanced in predicting ENSO events.

5 CONCLUSIONS

Based on zonal wind and vertical velocity data, a new Walker circulation index—OMGI—is constructed based on the difference between the average vertical velocity in the ascending area (100° E–140° E) and the sinking area (120°W–80°W).

The OMGI reaches the maximum in January and the minimum in May. These features correspond well with the seasonal characteristics of the WC. The interannual variation of the OMGI demonstrates typical decadal differences, showing the strongest WC in the 1970s and the weakest in the 1990s. In addition, the OMGI has a significant correlation with the SST in the equatorial Pacific. Their correlation coefficients are negative in the central and eastern equatorial Pacific and positive in the western equatorial Pacific. Therefore, the OMGI can characterize WC.

Importantly, the OMGI can also present substantial leading effect. The peak of the OMGI occurs ahead of ENSO events quite frequently. Among the 35 ENSO events, there are 19 ones when the OMGI peaks lead ENSO events (about 54.3%), with an average lead time of 2.6 months. For medium ENSO events, the lead proportion reaches 66.7%, with an average lead time of 3.1 months. For multi-peak ENSO events, the lead proportion reaches 69.2%, with an average lead time of 2.8 months. For El Niño and La Niña events, the lead proportions reach 56.3% and 52.6%, respectively. The average lead times are 4 months and 1.4 months, respectively.

***Acknowledgements*:** We thank the two experts for reviewing this paper and giving us some comments and thank Nanjing Hurricane Translation for reviewing the English language quality of this paper, too.

REFERENCES

[1] HASTENRATH S. Climate and Circulation of the Tropics [M]. Springer Netherlands, 1985, 45-50.

[2] GILL A E. Atmosphere-Ocean Dynamics [M]. Academic Press, 1982, 158-159.

[3] YANG Y B, CHEN L X. The coupled oscillation of air-sea system in the tropical Pacific Ocean [J]. Sci Atmos Sin, 1982, 6(1): 28-37 (in Chinese).

[4] BAYR T, DOMMENGET D, MARTIN T, et al. The eastward shift of the Walker Circulation in response to global warming and its relationship to ENSO variability [J]. Clim Dyn, 2014, 43(9-10): 2747-2763, https://doi.org/10.1007/s00382-014-2091-y.

[5] HAN W Q, GERALD A M, HU A X, et al. Decadal variability of the India and Pacific Walker cells since the 1960s: do they covary on decadal time scale? [J]. J Climate, 2017, 30: 8447-8467, https://doi. org / 10.1175 / JCLI-D-16-0783.1.

[6] SOHN B J, PARK S C. Strengthened tropical circulations in past three decades inferred from water vapor transport [J]. J Geophys Res Atmos, 2010, 115: D15112, https://doi.org/10.1029/2009JD013713.

[7] OLIVEIRA C P D, AÍMOLA L, AMBRIZZI T, et al. The influence of the regional Hadley and Walker Circulations on precipitation patterns over Africa in El Niño, La Niña, and neutral years [J]. Pure Appl Geophys, 2018, 175(5): 1-14, https://doi.org/10.1007/s00024-018-1782-4.

[8] YIM B, YEH S W, SOHN B J. ENSO-related precipitation and its statistical relationship with the Walker Circulation trend in CMIP5 AMIP Models [J]. Atmos, 2016, 7(2): 19-30, https://doi.org/10.3390/atmos7020019.

[9] SASAKI W, DOI T, RICHARDS K J, et al. The influence of ENSO on the equatorial Atlantic precipitation through the Walker circulation in a CGCM [J]. Clim Dyn, 2015, 44 (1-2): 191-202, https://doi.org/10.1007/s00382-014-2133-5.

[10] BJERKNES J. A possible response of the atmospheric Hadley circulation to equatorial anomalies of ocean temperature [J]. Tellus, 1966, 18: 820-829, https://doi.org/10.1111/j.2153-3490.1966.tb00303.x.

[11] BJERKNES J. Atmospheric teleconnections from the equatorial Pacific [J]. Mon Wea Rev, 1969, 97(3): 163-172. https://doi.org/10.1175/1520 -0493(1969) 097.

[12] PHILANDER S G. The response of equatorial oceans to a relaxation of the trade winds [J]. J Phys Oceanogr 1981, 11(2): 176-189, https://doi.org/10.1175/1520-0485(1981)011<0176:TROEOT>2.0.CO;2.

[13] WYRTKI K. El Niño-The dynamic response of the Pacific Ocean to atmospheric forcing [J]. J Phys Oceanogr, 1975, 5(4): 572-584, https://doi. org / 10.1175 / 1520-0485(1975)005<0572:ENTDRO>2.0.CO;2.

[14] WANG Y F, WANG B, OH J H. Impact of preceding El Niño on the East Asian summer atmosphere Circulation [J]. J Meteor Soc Japan, 2001, 79(1B): 575-588, https://doi.org/10.2151/jmsj.79.575.

[15] ANDERSON B T. Investigation of a large-scale mode of ocean-atmosphere variability and its relation to tropical Pacific sea surface temperature anomalies [J]. J Climate, 2004, 17(20): 1089-4098, https://doi. org / 10.1175 / 1520-0442(2004)017<4089:IOALMO>2.0.CO;2.

[16] TASAMBAY-SALAZAR M, ORTIZBEVIÁ M J, ALVAREZ-GARCÍA F J, et al. An estimation of ENSO predictability from its seasonal teleconnections [J]. Theor Appl Climatol, 2015, 122: 1-17, http://doi. org / 10.1007 / s00704-015-1596-6.

[17] WANG Y F, LUPO A R, QIN J. A Response in the ENSO cycle to an extratropical forcing mechanism during the El Niño to La Niña transition [J]. Tellus A, 2013, 65(1): 22431, https://doi.org/10.3402/tellusa.v65i0.22431.

[18] WANG Y F. The role of Pacific subtropical high belts in the ENSO cycle [J]. Tellus A, 2019, 71: 1656514, https://doi.org/10.1080/16000870.2019.1656514.

[19] WENG H, ASHOK K, BEHERA S K, et al. Impacts of recent El Niño Modoki on dry / wet conditions in the Pacific Rim during boreal summer [J]. Clim Dyn, 2007, 29(2-3): 113-129, https://doi. org / 10.1007 / s00382-007-0234-0.

[20] ZHANG W, JIN F F, TURNER A. Increasing autumn drought over southern China associated with ENSO regime shift [J]. Geophy Res Lett, 2014, 41(11): 4020-4026, https://doi.org/10.1002/2014GL060130.

[21] ZHI X F, YANG H, XU S W, et al. A comparative analysis of atmospheric and oceanic conditions before the occurrence of two types if El Niño events [J]. J Trop Meteor, 2019, 25(1): 34-45, https://doi. org / 10.16555 / j.1006-8775.2019.01.004.

[22] WANG Qin, LI Shuang-lin. Different summer rainfall anomaly patterns in northeast China Associated with two kinds of El Niño events [J]. J Trop Meteor, 2020, 26(2): 223-230, https://doi.org/10.46267/j.1006-8775.2020.020.

[23] SUN Z Q, XIANG J, GUAN Y P. Strengthening of the Pacific Walker Circulation in the recent decades [J]. J Trop Oceanog, 2016, 35(2): 19-29 (in Chinese).

[24] BO Y Q, WU H B. The intensity and location of Walker Circulation and its influence on ENSO [J]. Science and Technology Innovation Herald, 2008, (31): 5-7 (in Chinese).

[25] MA X M, ZHANG Y J. Walker Circulation has positive feedback effect to El Niño [J]. J Yunnan University, 2014, 36(S1): 103-111 (in Chinese).

[26] SMITH T M, REYNOLDS R W, PETERSON T C, et al. Improvements to NOAA's historical merged land-ocean surface temperature analysis (1880-2006) [J]. J Climate, 2008, 21(10): 2283-2296, https://doi. org / 10.1175 / 2007JCLI2100.1.

[27] ZHANG L, LI T. A simple analytical model for understanding the formation of sea surface temperature patterns under global warming [J]. J Climate, 2014, 27 (22): 8413-8421, https://doi. org / 10.1175 / JCLI-D-14-00346.1.

[28] ZHANG L, LI T. Relative roles of differential SST warming, uniform SST warming and land surface warming in determining the Walker circulation changes under global warming [J]. Clim Dyn, 2016, 48(3-4): 1-11, https://doi.org/10.1007/s00382-016-3123-6.

[29] YUE R H, XU H M. Variations of the spring equatorial Indian Ocean zonal-vertical circulation and its correlation with the Walker Circulation [J]. Chin J Atmos Sci, 2016, 41(1): 213-226 (in Chinese).

[30] SOHN B J, YEH S W, SCHMETZ J, et al. Observational evidences of Walker circulation change over the last 30 years contracting with GCM results [J]. Clim Dyn, 2013, 40(7/8): 1721-1732, https://doi.org/10.1007/s00382-012-

1484-z.

[31] SUN S J, LI D L. Variability in the western Pacific subtropical high and its relationship with sea temperature variation considering the background of climate warming over the past 60 years [J]. J Trop Meteor, 2018, 24(4): 468-480, https://doi. org / 10.16555 / j. 1006-8775.2018.04.006.

[32] YUAN S, XU J J, PAN Y S. Diversity of super El Niño events and their impact on east summer monsoon precipitation[J]. J Trop Meteor, 2019, 35(3): 379-389 (in Chinese).

[33] ZHANG L, LI T. Relative roles of differential SST warming, uniform SST warming and land surface warming in determining the Walker circulation changes under global warming [J]. Clim Dyn, 2017, 48: 987-997, https://doi.org/10.1007/s00382-016-3123-6.

[34] ANA C V F, LUIS A, TÉRCIO A, et al. Changes in intensity if the regional Hadley cell in Indian Ocean and its impacts on surrounding regions [J]. Meteorol Atmos Phys, 2017, 129: 229-246, https://doi.org/10.1007/s00703-016-0477-6.

Citation: SHI Dan-dan, RONG Yan-shu, LYU Xing-yue, et al. A new index about the Walker circulation [J]. J Trop Meteor, 2020, 26 (3): 311-320, https://doi.org/10.16555/j.1006-8775.2020.028.